processes

MDPI

Article

The Engineering of Porous Silica and Hollow Silica Nanoparticles to Enhance Drug-loading Capacity

Ngoc-Tram Nguyen-Thi [1,2], Linh Phuong Pham Tran [3], Ngoc Thuy Trang Le [2,3], Minh-Tri Cao [1], The-Nam Tran [1], Ngoc Tung Nguyen [2,4], Cong Hao Nguyen [2,3], Dai-Hai Nguyen [2,3], Van Thai Than [5,6,*], Quang Tri Le [7] and Nguyen Quang Trung [8,*]

1 Tra Vinh University, No. 126, Nguyen Thien Thanh, Ward 5, Tra Vinh city 940000, Vietnam
2 Graduate University of Science and Technology, Vietnam Academy of Science and Technology, Hanoi 100000, Vietnam
3 Institute of Applied Materials Science, Vietnam Academy of Science and Technology, 01 TL29, District 12, Ho Chi Minh City 700000, Vietnam
4 Center for Research and Technology Transfer, Vietnam Academy of Science and Technology, Hanoi 100000, Vietnam
5 NTT Hi-Tech Institute, Nguyen Tat Thanh University, Ho Chi Minh City 700000, Vietnam
6 Center of Excellence for Functional Polymers and NanoEngineering, Nguyen Tat Thanh University, Ho Chi Minh City 700000, Vietnam
7 Department of Orthopedic, 7A Military Hospital, 466 Nguyen Trai Street, Ward 8, District 5, 72706, Ho Chi Minh City 700000, Vietnam
8 Nghe An Oncology Hospital, Vinh City 460000, Vietnam
* Correspondence: tvthai@ntt.edu.vn (V.T.T.); nqtrung8910@gmail.com (N.Q.T.)

Received: 23 June 2019; Accepted: 29 August 2019; Published: 4 November 2019

check for updates

Abstract: As a promising candidate for expanding the capacity of drug loading in silica nanoplatforms, hollow mesoporous silica nanoparticles (HMSNs) are gaining increasing attention. In this study, porous nanosilica (PNS) and HMSNs were prepared by the sol-gel method and template assisted method, then further used for Rhodamine (RhB) loading. To characterize the as-synthesized nanocarriers, a number of techniques, including X-ray diffraction (XRD), transmission electron microscopy (TEM), nitrogen absorption-desorption isotherms, dynamic light scattering (DLS), thermogravimetric analysis (TGA), and Fourier transform infrared spectroscopy (FTIR) were employed. The size of HMSN nanoparticles in aqueous solution averaged 134.0 ± 0.3 nm, which could be adjusted by minor changes during synthesis, whereas that of PNS nanoparticles was 63.4 ± 0.6 nm. In addition, the encapsulation of RhB into HMSN nanoparticles to form RhB-loaded nanocarriers (RhB/HMSN) was successful, achieving high loading efficiency (51.67% ± 0.11%). This was significantly higher than that of RhB-loaded PNS (RhB/PNS) (12.24% ± 0.24%). Similarly, RhB/HMSN also possessed a higher RhB loading content (10.44% ± 0.02%) compared to RhB/PNS (2.90% ± 0.05%). From those results, it is suggested that prepared HMSN nanocarriers may act as high-capacity carriers in drug delivery applications.

Keywords: hollow mesoporous silica; porous silica; high drug loading capacity; nanoparticles; drug delivery system

1. Introduction

Various advantages of porous nanosilica (PNS), such as a large surface area, chemical and thermal stability, high biocompatibility and biodegradability, and readiness for surface functionalization, have made it an excellent nanocarrier system for drug delivery applications [1–4]. Due to the unique porous structure of the PNS nanocarriers, anticancer drugs could be effectively encapsulated, and protected from temperature variation and pH-induced enzymatic degradation of the surrounding media [5–7]. However, concerns about toxicity of the carriers have been expressed [8,9]. As a result, the reduction in toxicity of the nanocarrier by improving the drug loading capacity of silica nanoplatforms is of great significance.

A sub class of PNS, hollow mesoporous silica nanoparticles (HMSNs), is a structure of a mesoporous silica shell possessing a large cavity at the core of the particle [10–13], offering a potential solution to the problem of low capacity. It can be said that the HMSN was developed bearing in mind the importance of PNS applications in drug and bio-sensing agents' delivery. The large compartment inside each HMSN vastly increases their drug loading capacity and pore volume compared to conventional PNS [14,15]. Accordingly, it can be theoretically concluded that a lower amount of HMSNs is needed to deliver the same load of drug, and thus to achieve the desired therapeutic effect by comparison with that of PNS, hence minimizing the potential accumulation of foreign materials in the host. Moreover, HMSNs retain the property of a readily conjugatable surface, making them an increasingly recognized platform for fabricating stealth mechanisms and stimuli-responsive functionalization [16–21].

In a recent report, a HMSNs-b- cyclodextrin (CD) nanocarrier was formed by grafting 3-(3,4-dihydroxypheneyl) propionic acid (DHPA)-functionalized beta-cyclodextrin (b-CD) onto the surface of HMSNs, and was further anchored with polyethylene glycol (PEG)-conjugated adamantane (Ada) via host–guest interaction for the delivery of doxorubicin (DOX). It was revealed from thermogravimetric analysis (TGA) results that the DOX encapsulation efficiency of the HMSNs-b-CD/Ada-PEG carrier reached around 10 wt% of DOX. This figure was greater than that of PNS of a similar size, at approximately 5 wt%, which could be explained by the hollow cavity of HMSNs [22]. In another study, positively charged CD_{PEI} nanoparticles were grafted on the pore openings of HMSNs through disulfide bonds. The carrier was later then loaded with DOX and grafted with hyaluronic acid (HA) to yield a more complex structure—DOX/HMSN-SS-CD_{PEI}@HA, resulting a drug loading efficiency of 30.5%. Compared to the DOX-loaded PNS, the HMSN-SS-CD_{PEI}@HA nanoparticles had higher loading capacity and excellent biocompatibility. These advantages are generally due to mesoporous structure, high specific surface area, and particularly, the hollow cavity of the HMNS nanoparticle, suggesting its use as a high capacity nanocarrier for drug delivery [23].

Among the various methodologies to fabricate HMSN, the template assisted method is one of the most controllable methods, regardless of a wide range of template-free routes that have emerged recently [10,11,24]. With regard to template assisted fabrication, the hard template in the form of a solid SiO_2 core ($sSiO_2$) is first synthesized via a modified Stöber method. Afterwards, the sol-gel process of tetrathylorthorsilicates (TEOS) catalyzed by acid or base in the presence of hexadecyltrimethylammnomium bromide (CTAB) was performed to form a controllable PNS layer, which was then used to coat the $sSiO_2$ spheres, prepared as mentioned. The silica cores were then separated through selective etching in a suitable solvent, Na_2CO_3, for etching at a high temperature [25].

In this study, a process for synthesizing PNS and HMSN nanocarriers was reported. The as-synthesized systems were compared for Rhodamine (RhB) loading capacity and efficiency. Both carriers were characterized by a number of techniques, including X-ray diffraction (XRD), transmission electron microscopy (TEM), nitrogen absorption-desorption isotherms, dynamic light scattering (DLS), thermogravimetric analysis (TGA), and Fourier transform infrared spectroscopy (FTIR), respectively to evaluate the crystallinity, morphology, BET surface area, size and size distribution, and composition of the materials.

2. Materials and Methods

2.1. Materials

Reagent grade chemicals, including Tetraethyl orthosilicate (TEOS, 98%), Cetyltrimethylammonium bromide (CTAB, 99%), and Rhodamine B were commercially obtained from Sigma-Aldrich (St. Louis, MO, USA), Merck (USA), and HiMedia (India), respectively. Ammonia solution (NH_3 (aq), 28%) and ethanol were purchased from Scharlau (Barcelona, Spain). All chemicals were used as received.

2.2. Preparation of PNS

The sol gel technique was used to prepare PNS in which a TEOS, CTAB, ethanol, and water, act as the silicone source, structure-directing agent, solvent, and reactant, respectively. The TEOS was hydrolyzed and condensed with ammonia (NH_3) (Figure 1a). Initially, 2.8% NH_3 solution (0.07 M), deionized water (deH_2O), ethanol (2.2 M), and CTAB (2.6 g) were mixed together at 60 °C with a stir-bar for 30 min. Afterwards, the solution was introduced drop-wise with TEOS (0.4 M) for 2 h under stirring at 60 °C, followed by dialysis using MWCO 12–14 kDa membrane (Spectrum Laboratories, Inc., Rancho Dominguez, CA 90220, USA) against an acetic acid (2 M)/ethanol (1:1, *v/v*) solution and then with deH_2O at room temperature. A solid product was finally obtained by calcination at 500 °C for 24 h.

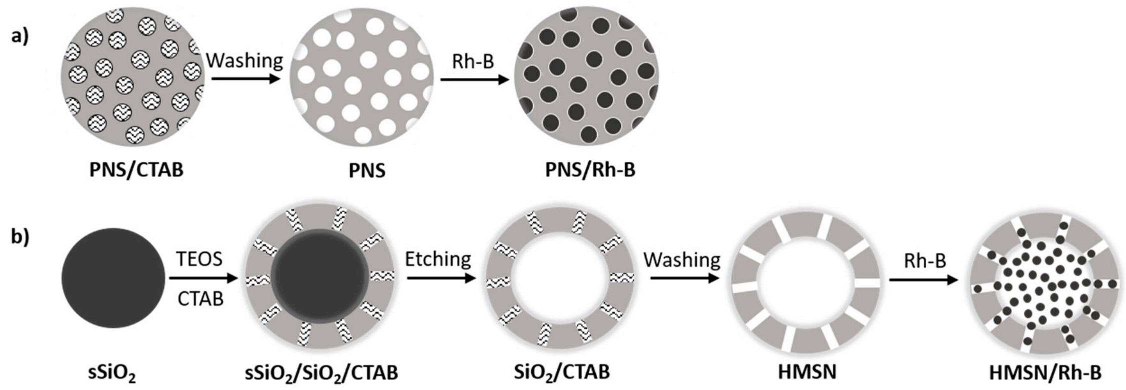

Figure 1. Schematic representation of the formation of porous nanosilica (PNS) (**a**) and hollow mesoporous silica nanoparticles (HMSNs) (**b**).

2.3. Preparation of HMSNs

HMSNs were prepared via a previously reported procedure with minor modification, including three main stages, as shown in Figure 1b [12,26]. The synthesis commenced with the preparation of hard templates of $sSiO_2$ spheres via the Stöber method with modifications [27]. In detail, ethanol (13.5 M), deH_2O (6.0 M), and ammonium hydroxide (0.38 M) were mixed together under constant stirring at 50 °C for 30 min. The resultant solution was then introduced with TEOS solution (0.29 M) at room temperature and subject to another 6h of stirring. Afterwards, dialysis with an MWCO 12–14 kDa membrane and freeze-drying took place to obtain the final solution. In the second step, a structure was formed by coating a thickness-controlled PNS layer on each $sSiO_2$ using CTAB as the organic co-templates [28]. The core@shell structure was denoted as $sSiO_2/SiO_2$/CTAB. Briefly, CTAB (0.05 M) was dissolved in deH_2O under magnetic stirring at room temperature for 15 min. $sSiO_2$ solution (5 mL) was added into the CTAB solution using a magnetic stir bar for 30 min at 50 °C, followed by the addition of a mixture of ethanol/ammonia solution (1.43:0.05, M/M). TEOS solution (0.27) was added into the above mixture under magnetic stirring at 50 °C for 6 h and the obtained solution was dialyzed against deH_2O (MWCO 12–14 kDa), which was changed 5 or 6 times per day, for 4 days. In the third step, the prepared $sSiO_2/SiO_2$/CTAB and free CTAB were mixed with an aqueous Na_2CO_3 solution (0.2 M) for 9 h under stirring at 50 °C. HMSN spheres, obtained by freeze-drying the above mixture (EyeLA FDU-1200, −38.3 °C, 29.5 Pa), were soaked in acetic acid (2 M)/ethanol (1:1, *v/v*) solution over 24 h and had the CTAB template removed by washing with deH_2O several times.

2.4. Characterization

A Bruker D2 Phaser diffractometer (Germany) with Cu/Kα radiation at a scanning rate of 4°/min (λ = 0.154056 nm, 40 kV, 40 mA) was employed to perform XRD measurements. PNS, $sSiO_2$, $sSiO_2/SiO_2$/CTAB, and HMSNs were morphologically characterized and measured for size via TEM using JEM-1400 (JEOL, Tokyo, Japan) operating at an accelerating voltage of 300 kV. To prepare the sample for TEM analysis, one drop of each solution was added in deH_2O (1 mg/mL) and placed onto a carbon-copper grid (300-mesh, Ted Pella, Inc., Redding, CA, USA), which was then subject to air-drying for 10 min.

A TRISTAR 3000 instrument (Micromeritics, Norcross, GA, USA) operating at 77 K under continuous adsorption conditions was employed to measure N_2 adsorption–desorption isotherms. Before being analyzed, samples were subject to degassing at 103 Torr at 110 °C for 16 h. The size distribution of pores was derived via the Barrett–Joyner–Halenda method from the desorption branch of the nitrogen isotherm. The pore volume was taken at P/P_o-0.97 single point.

To perform TGA, a TGAnalyzer (Perkin Elmer Pyris 1, Perkin Elmer, Hopkinton, MA, USA) operating at a heating rate of 20 °C/min in a nitrogen flow from 100 °C to 800 °C was employed. The measurement of the surface charge of PNS and HMSN was performed at 37 °C using a Zetasizer Nano ZS (ZEN 3600, Malvern Instruments, Malvern, UK), equipped with a 532 nm wavelength. UV-Vis spectroscopy (Shimadzu, Kyoto, Japan) with a wavelength of 544 nm was used to determine the loading content of HMNS with RhB.

2.5. Preparation of RhB/PNS and RhB/HMSN

The equilibrium dialysis method, which was described previously, was used to load RhB into PNS and HMSN [1]. Briefly, solutions with either PNS or HMSN were created by adding 16 mg of the carrier into RhB solution (10 µg/mL). These solutions were stirred for 12 h to allow the encapsulation of RhB into the carriers. Unloaded RhB in the solutions was then removed by dialysis. In the dialysis solution, the content of unloaded RhB ($W_{U.RhB}$) was measured via the UV-Vis absorbance method, in which the standard curve was established by dissolving bare RhB in deH_2O to create multiple solutions with pre-specified concentrations (0–5 µg/mL). The recording of absorbance of the standard and dialysis solutions were performed with a V-750 UV/Vis spectrophotometer (Jasco Co., Tokyo, Japan). Based on the standard curve, which explains the relationship between RhB content and absorbance, and the absorbance results, the contents of RhB in the samples were determined. RhB loading efficiency (LE) and loading capacity (LC) were calculated as follows:

$$\mathrm{LE}(\%) = \frac{(100 - W_{U.RhB})}{100} \times 100$$
$$\mathrm{LC}(\%) = \frac{(100 - W_{U.RhB})}{W_{PNS\,or\,HMSN} + 100 - W_{U.RhB}} \times 100$$

In which the 100 (mg) was the initial amount of RhB for loading experiments. $W_{U.RhB}$ and $W_{PNS\ or\ HMSN}$ are the content of unloaded RhB in the dialysis solution and the dried weight of the nanocarrier respectively.

2.6. Statistical Analysis

Microsoft® Excel was used to process the data. The results were expressed as mean ± standard deviation.

3. Result and Discussion

Figure 1 shows the synthesis of PNS and HMSN following a previously described procedure [26]. While Figure 1a represented the procedure of synthesizing PNS, Figure 1b illustrated three main steps for preparation of HMSN, including the preparations of the $sSiO_2$ core, mesoporous shell ($sSiO_2/SiO_2$/CTAB), and hollow core (HMSN). The successful preparation of PNS and HMSN was indicated by FTIR spectra shown in Figure 2. In Figure 2a, a band at 1640 cm^{-1} was attributed to the OH stretching vibration of water molecules present in PNS. Stretching vibrations of Si–O–Si, Si–OH, and Si–O could also be assigned to strong peaks at around 1089, 973, and 836 cm^{-1}, which are typical peaks of silica nanoparticles. The broad band observed at around 3444 cm^{-1} was associated with OH stretching frequency for the silanol group. These aforementioned peaks were also present in the spectrum of HMSN.

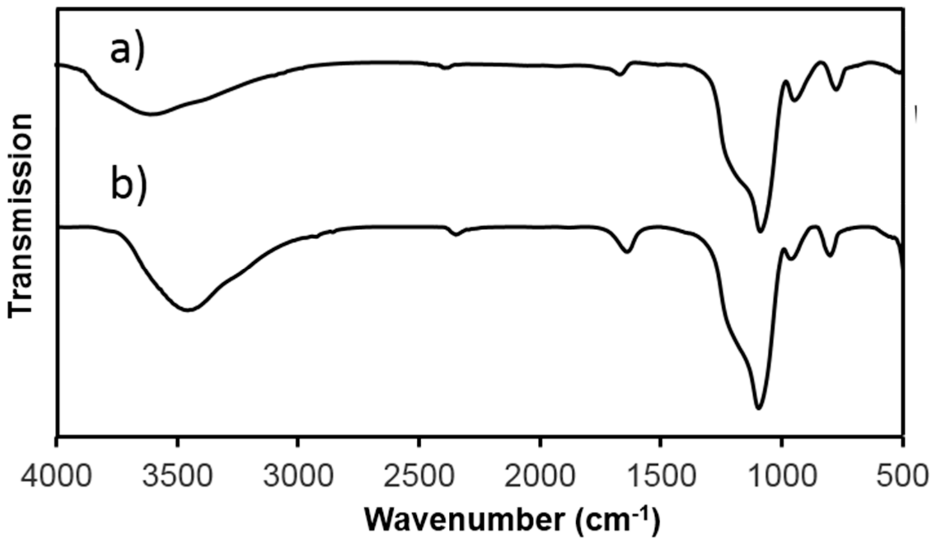

Figure 2. The FTIR spectra of PNS (**a**) and HMSN (**b**).

The TGA curves of PNS (a) and HMSN (b) are shown in Figure 3, in which the temperature was elevated to 800 °C at a constant rate of 10 °C/min. As high temperature leads to decomposition and vaporization of an organic fraction, inorganic remainders are often found at the end of the analysis. Generally, a pattern of mass depreciation could be observed for both PNS and HMSN. First, in the temperature range of lower than 200 °C, the removal of physically adsorbed water produced by hydrolysis of the precursors and the solvent employed during the synthesis took place. In the second range of 200–600 °C, residual organic product (CTAB) from the decomposition of the precursors was lost and the dehydroxylation of silanol (SiOH) groups from the silica surface occurred. In this phase, the weight loss of PNS was approximately 30%, whereas that of HMSN was only 13%, indicating that a small amount of CTAB may have remained in the HMSN nanoparticles.

The prepared nanoparticles were further characterized by TEM for morphological examination and size measurement. Figure 4 revealed the average diameter of PNS to be 63.4 ± 0.6 nm, and $sSiO_2$ to be 104.0 ± 0.7 nm (Figure 4a,b). As reported by Chen el al., the size of $sSiO_2$ was essential in influencing the size of hollow core [11]. Different hollow structures can be obtained in the sizing process of $sSiO_2$ by altering the reagent ratio in the initial stage. In the next step, by coating a mesoporous silica layer, the $sSiO_2/SiO_2$/CTAB and HMSN nanoparticles possessed spherical shapes, with significantly increased particle sizes, which were 167 ± 0.5 nm and 134 ± 0.3 nm for $sSiO_2/SiO_2$/CTAB and HMSN, respectively (Figure 4c). This could be explained by the binding of the outer PNS layer (Figure 1b), in which case the thickness and pore size of the mesoporous shell with the biodegradable property could be modified by using different organic solvents, adjusting concentration of TEOS, and reaction time [11]. In the last step aiming at selectively etching the solid silica core and protecting the integrity of silica shell, the absorption of positively charged CTAB ($CTAB^+$) onto the surface of $sSiO_2/SiO_2$/CTAB took place via electronic attraction to keep the shell intact. After commencing, this mechanism was stimulated by the Na_2CO_3 existing in the solution, CTAB in the PNS shell, and free CTAB in the media. Following the etching process, the acid acetic acid (2 M)/ethanol (1:1, *v/v*) solution was used to remove CTAB from the mesopores.

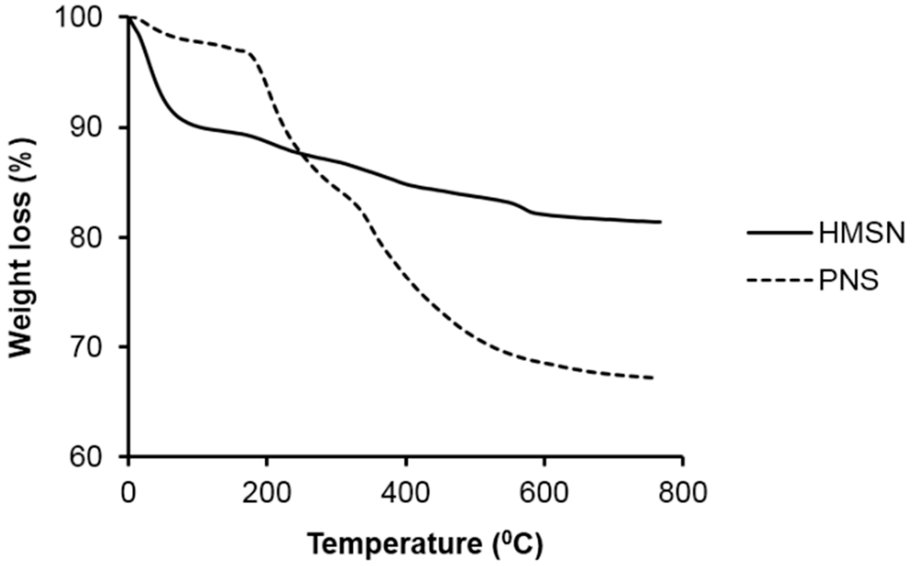

Figure 3. Thermogravimetry analysis for PNS (**a**) and HMSN (**b**).

In the blood circulation, it was suggested that the extravasation and renal clearance of nanoparticles of less than 10 nm in diameter are more expedited than those of larger nanoparticles (<200 nm), which are likely to be retained for a longer period [29,30]. Accordingly, the achieved size of synthesized HMSN products have the potential to allow the particles to bypass early clearance through kidney and vascular leakage.

Figure 5 shows the XRD patterns of PNS (a) and HMSN (b). As shown, the broad XRD reflection peaks of PNS (2θ = 21.1°) and HMSN (2θ = 23.0°) both indicate the amorphous nature of silica nanoparticles [31]. In addition, apart from a small amorphous bump at 37° in the PNS sample that could be attributed to trace CTAB left after calcination, no considerable difference was found between the two XRD patterns of PNS and HMSN, indicating that these nanoparticles likely have similar structures.

In addition, the porosities of the prepared PNS and HMSNs were evaluated by the N_2 adsorption-desorption technique. The results are presented in Figure 6b. It was noticed that the isotherms of both PNS and HMSN belong to the Langmuir type IV, characterized by a hysteresis loop, suggesting that both materials possess a mesoporous structure [32]. The hysteresis loops indicated the capillary condensation associated with mesopores, which occurred much more rapidly at higher pressure in PNS than in HMSN. Another difference between the materials is the type of the hysteresis loop, with PNS being H1, with the adsorption and desorption branches almost vertical and parallel at relative pressures of 0.9 to 1.0. This type of loop is associated with uniform particles and narrow distribution of pore size [33], while the H4 loop of HMSN—in which the adsorption and desorption branches remain nearly horizontal and parallel over a wide range of pressure—indicates irregular but parallel, open-ended, and slit-like pores, with connectivity between intragranular pores, and it indicates the existence of some micropores [33]. The N_2 adsorption percentage of HMSN over 60 min was almost 96%, which was higher than that of PNS (84%). This phenomenon could be explained by the hollow cavity of HMSN. The specific area and pore volume of HMSNs were 983.7 m^2/g and 2.33 cm^3/g, respectively. These figures were starkly contrasted by values found in PNS, which were 155.2 m^2/g and 8.75 cm^3/g, respectively, indicating that the prepared HMSN could be a potential carrier for bioactive molecules, with a high capacity. Having said that, further investigations on strategies to modify the surface of HMSN are still required to improve the controllability of this system, due to its similar nature to silica nanoparticles, whose availability for functionalization is abundant [4,34].

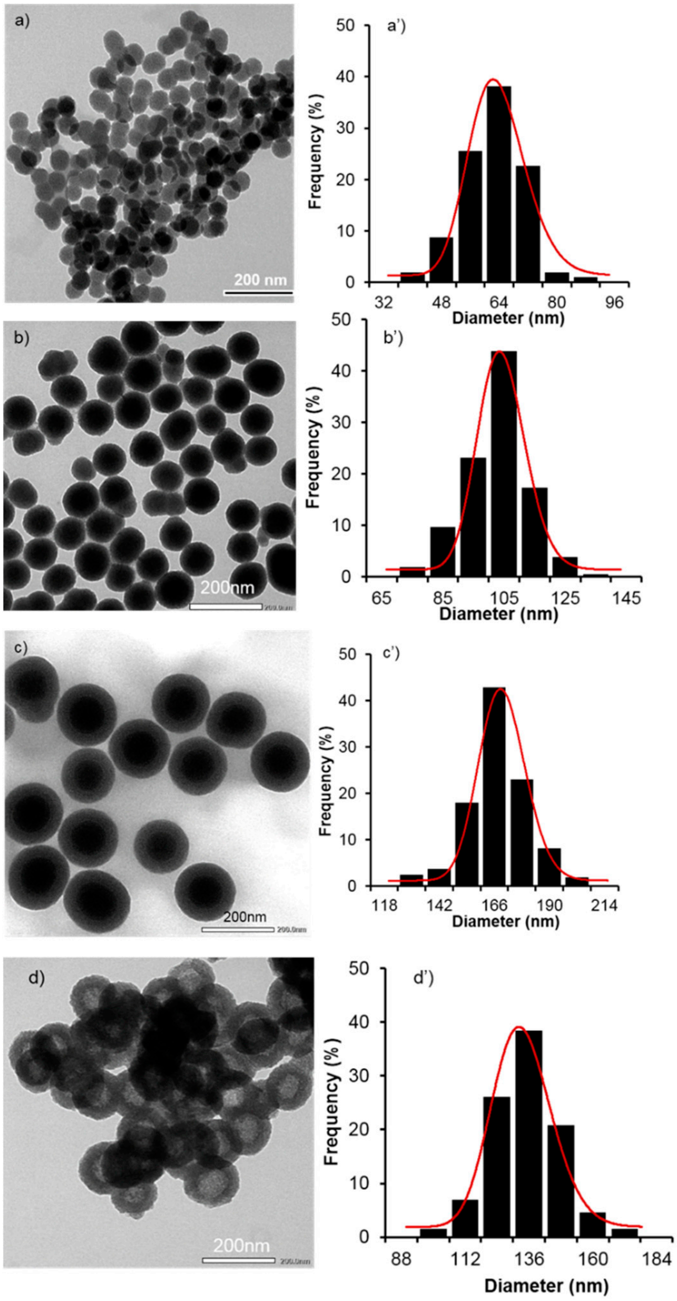

Figure 4. TEM images and the particle size distribution of PNS (**a**,**a'**), $sSiO_2$ (**b**,**b'**), $sSiO_2/SiO_2$/CTAB (**c**,**c'**), and HMSN (**d**,**d'**), respectively.

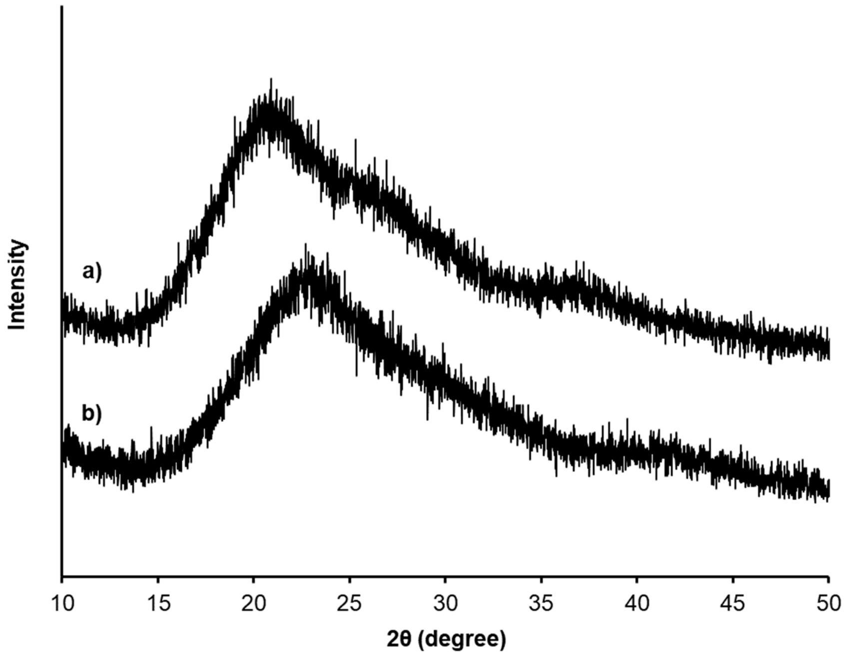

Figure 5. XRD patterns of PNS (**a**) and HMSN (**b**).

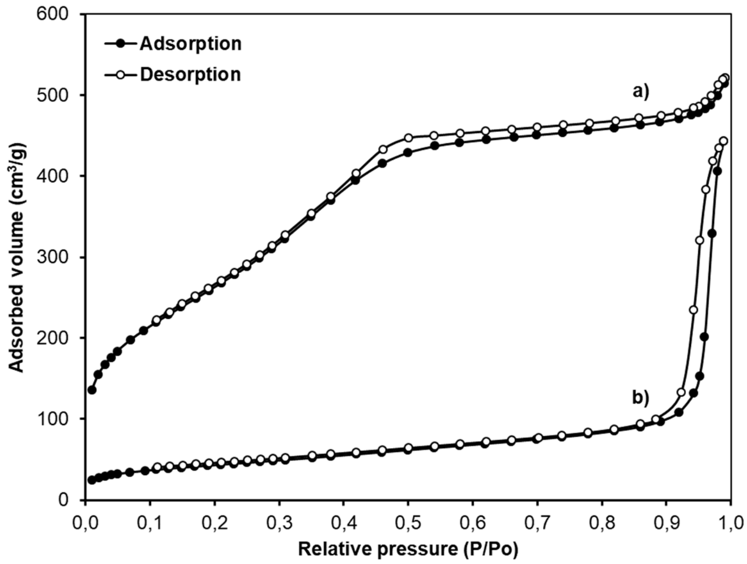

Figure 6. Nitrogen adsorption–desorption isotherms of HMSN (**a**) and PNS (**b**).

The surface charge of the prepared PNS, $sSiO_2$, $sSiO_2$/PNS(CTAB), and HMSN nanoparticles were characterized by zeta potential measurements. Results for the latter three are presented in Figure 7a. Not only does the zeta potential data expresses the stability of $sSiO_2$ nanoparticles' dispersion in water, the technique has also been employed to elucidate the adsorption mechanisms of drugs and biological ligands on the surface of $sSiO_2$ nanoparticles. It is stated that the absolute value of zeta potential is positively associated with the stability of colloidal systems. An absolute value of higher than 30 mV indicates a stable suspension [35]. The surface charges of the $sSiO_2$ and PNS were found to be −43.3 ± 0.87 mV and −44.53 ± 0.23 mV, respectively, in this study. The highly negative charges of $sSiO_2$ and PNS nanoparticles were attributed to the ionization of –OH on the surfaces of silica in the ethanol solutions. However, the zeta potential of $sSiO_2$/PNS(CTAB) increased dramatically to 32.5 ± 0.66 mV, for the adsorption of CTA cations (CTA^+) in CTAB on the $sSiO_2$ surface, via electronic attraction. By contrast, there was then a steep decrease in the zeta potential of HMSN, reaching

−25.45 ± 0.07 mV, different to $sSiO_2$/PNS(CTAB) due to the absence of CTA^+ after the etching process. Moreover, an investigation into the stability of the particles in aqueous solution is also presented in Figure 7b, which demonstrated a stable surface charge after 48 h. These results suggest a potential application of PNS and HMSN nanoparticles for drug delivery systems with high stability.

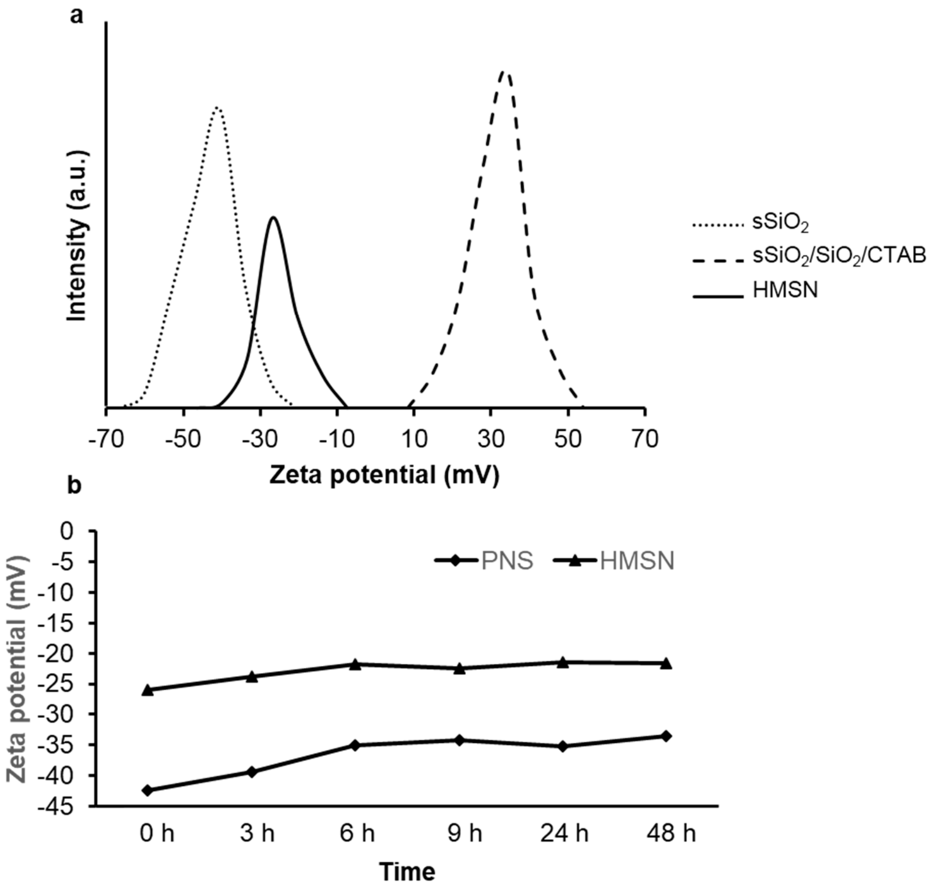

Figure 7. (**a**) Zeta potential of $sSiO_2$, $sSiO_2/SiO_2$/CTAB, and HMSN; (**b**) Zeta potential of PNS and HMSN in solutions over the course of 48 h.

Drug loading efficiency and capacity are considered to be essential in any drug delivery system design, since they play a direct role in the therapeutic activity of the system [36]. A high loading capacity is also desirable for our rationale of minimizing the dose-dependent toxicity of the delivery system. In our case, the LE, indirectly derived from the content of non-encapsulated RhB, of PNS and HMSN were 12.24% and 51.67%, respectively. The lower RhB LE in RhB/PNS nanocarriers was attributed to their non-hollow structure. In contrast, RhB/HMSN nanocarriers possessed a significantly higher LE due to the hollow nature of the HMSN's cavity, leading to a significantly improved drug loading capacity. Similarly, RhB/HMSN also showed a higher LC (10.44%) compared to RhB/PNS (2.9%). Therefore, it is suggested that the introduction of a hollow form may improve the LE and LC of HMSN nanoparticles, assisting the tumor-targeted delivery and therapeutic result of a drug that is loaded into HMSN nanocarriers.

4. Conclusions

The present study has reported a successful preparation attempt of PNS and HMSN nanoparticles via sol-gel method. The formed PNS and HMSN existed in spherical shapes with average particle sizes of 63.4 ± 0.6 nm and 134.0 ± 0.3 nm, and were proved to be potential carriers for anticancer drugs. The encapsulation of RhB into the HMSN nanoparticles achieved the LE of 51.67%. The high LE achieved could be a contributing factor to the reduction of dose-dependent toxicity in drug delivery with nanocarriers. However, further studies are required to further improve the HMSN system, especially regarding surface modification for stealth delivery, and to offer more sustainability in cargo release from this system.

Author Contributions: Conceptualization, investigation, and data analysis, N.-T.N.-T.; data curation, writing—original draft preparation, and visualization, L.P.P.T. and N.T.T.L.; writing—reviewing and editing, M.-T.C., T.-N.T., N.T.N., C.H.N.; supervision and project administration, D.-H.N., V.T.T., Q.T.L., and N.Q.T.

Funding: This research was funded by Tra Vinh University (grant number 177/HD.HDKH-DHTV).

Conflicts of Interest: The authors declare no conflict of interest.

References

1. Vo, U.V.; Nguyen, C.K.; Nguyen, V.C.; Tran, T.V.; Thi, B.Y.T.; Nguyen, D.H. Gelatin-poly (ethylene glycol) methyl ether-functionalized porous Nanosilica for efficient doxorubicin delivery. *J. Polym. Res.* **2019**, *26*, 6. [CrossRef]
2. Lu, J.; Liong, M.; Zink, J.; Tamanoi, F. Mesoporous Silica Nanoparticles as a Delivery System for Hydrophobic Anticancer Drugs. *Small* **2007**, *3*, 1341–1346. [CrossRef]
3. Slowing, I.I.; Trewyn, B.; Giri, S.; Lin, V.S.Y. Mesoporous silica nanoparticles for drug delivery and biosensing applications. *Adv. Funct. Mater.* **2007**, *17*, 1225–1236. [CrossRef]
4. Thi, T.T.H.; Cao, V.D.; Nguyen, T.N.Q.; Hoang, D.T.; Ngo, V.C.; Nguyen, D.H. Functionalized mesoporous silica nanoparticles and biomedical applications. *Mater. Sci. Eng. C* **2019**, *99*, 631–656.
5. Bao, B.Q.; Le, N.H.; Nguyen, D.H.T.; Tran, T.V.; Pham, L.P.T.; Bach, L.G.; Ho, H.M.; Nguyen, T.H.; Nguyen, D.H. Evolution and present scenario of multifunctionalized mesoporous nanosilica platform: A mini review. *Mater. Sci. Eng. C* **2018**, *91*, 912–928. [CrossRef] [PubMed]
6. Slowing, I.I.; Vivero-Escoto, J.; Wu, C.W.; Lin, V.S.Y. Mesoporous silica nanoparticles as controlled release drug delivery and gene transfection carriers. *Adv. Drug Deliv. Rev.* **2008**, *60*, 1278–1288. [CrossRef] [PubMed]
7. Tang, F.; Li, L.; Chen, D. Mesoporous silica nanoparticles: Synthesis, biocompatibility and drug delivery. *Adv. Mater.* **2012**, *24*, 1504–1534. [CrossRef] [PubMed]
8. Chauhan, S.; Manivasagam, G.; Kumar, P.; Ambasta, R.K. Cellular Toxicity of Mesoporous Silica Nanoparticle in SHSY5Y and BMMNCs Cell. *Pharm. Nanotechnol.* **2018**, *6*, 245–252. [CrossRef] [PubMed]
9. Murugadoss, S.; Lison, D.; Godderis, L.; Brule, S.V.D.; Mast, J.; Brassinne, F.; Sebaihi, N.; Hoet, P.H. Toxicology of silica nanoparticles: An update. *Arch. Toxicol.* **2017**, *91*, 2967–3010. [CrossRef] [PubMed]
10. Tsou, C.J.; Hung, Y.; Mou, C.Y. Hollow mesoporous silica nanoparticles with tunable shell thickness and pore size distribution for application as broad-ranging pH nanosensor. *Microporous Mesoporous Mater.* **2014**, *190*, 181–188. [CrossRef]
11. Chen, F.; Hong, H.; Shi, S.; Goel, S.; Valdovinos, H.F.; Hernandez, R.; Theuer, C.P.; Barnhart, T.E.; Cai, W. Engineering of Hollow Mesoporous Silica Nanoparticles for Remarkably Enhanced Tumor Active Targeting Efficacy. *Sci. Rep.* **2014**, *4*, 5080. [CrossRef] [PubMed]
12. Farsangi, Z.J.; Rezayat, S.M.; Beitollahi, A.; Sarkar, S.; Jaafari, M.; Amani, A. Hollow Mesoporous Silica Nanoparticles (HMSNs) Synthesis and in vitro Evaluation of Cisplatin Delivery. *J. Nanoanal.* **2016**, *3*, 120–127.
13. Ghasemi, S.; Farsangi, Z.; Beitollahi, A.; Mirkazemi, S.M.; Rezayat, M.; Sarkar, S. Synthesis of Hollow Mesoporous Silica (HMS) nanoparticles as a candidate for sulfasalazine drug loading. *Ceram. Int.* **2017**, *43*, 11225–11232. [CrossRef]
14. Zhu, Y.; Fang, Y.; Borchardt, L.; Kaskel, S. PEGylated hollow mesoporous silica nanoparticles as potential drug delivery vehicles. *Microporous Mesoporous Mater.* **2011**, *141*, 199–206. [CrossRef]
15. Shi, S.; Chen, F.; Cai, W. Biomedical applications of functionalized hollow mesoporous silica nanoparticles: Focusing on molecular imaging. *Nanomedicine* **2013**, *8*, 2027–2039. [CrossRef]
16. Zhu, Y.; Shi, J.; Shen, W.; Dong, X.; Feng, J.; Ruan, M.; Li, Y. Stimuli-Responsive Controlled Drug Release from a Hollow Mesoporous Silica Sphere/Polyelectrolyte Multilayer Core–Shell Structure. *Angew. Chem. Int. Edit.* **2005**, *44*, 5213–5217. [CrossRef]
17. Mei, X.; Yang, S.; Chen, D.; Li, N.; Li, H.; Xu, Q.; Ge, J.; Lu, J. Light-triggered reversible assemblies of azobenzene-containing amphiphilic copolymer with β-cyclodextrin-modified hollow mesoporous silica nanoparticles for controlled drug release. *Chem. Commun.* **2012**, *48*, 10010–10012. [CrossRef]

18. Ma, X.; Zhao, Y.; Ng, K.W.; Zhao, Y. Integrated hollow mesoporous silica nanoparticles for target drug/siRNA co-delivery. *Chem. A Eur. J.* **2013**, *19*, 15593–15603. [CrossRef]
19. Yang, Y.; Guo, X.; Wei, K.; Wang, L.; Yang, D.; Lai, L.; Cheng, M.; Liu, Q. Synthesis and drug-loading properties of folic acid-modified superparamagnetic Fe_3O_4 hollow microsphere core/mesoporous SiO_2 shell composite particles. *J. Nanopart. Res.* **2014**, *16*, 2210. [CrossRef]
20. Patil, P.B.; Karade, V.; Waifalkar, P.P.; Sahoo, S.C.; Kollu, P.; Nimbalkar, M.; Chougale, A.D.; Patil, P.S. Functionalization of magnetic hollow spheres with 3-Aminopropyl) triethoxysilane (APTES) for controlled drug release. *IEEE Trans. Magn.* **2017**, *53*, 1–4. [CrossRef]
21. Vo, U.V.; Tran, T.V.; Nguyen, D.M.T.; Nguyen, C.K.; Thi, N.T.N.; Nguyen, D.H. Effective pH-responsive hydrazine-modified silica for doxorubicin delivery. *Asian J. Med. Health* **2017**, *4*, 1–7. [CrossRef]
22. Liu, J.; Luo, Z.; Zhang, J.; Luo, T.; Zhou, J.; Zhao, X.; Cai, K. Hollow mesoporous silica nanoparticles facilitated drug delivery via cascade pH stimuli in tumor microenvironment for tumor therapy. *Biomaterials* **2016**, *83*, 51–65. [CrossRef] [PubMed]
23. Zhao, Q.; Wang, S.; Yang, Y.; Li, X.; Di, D.; Zhang, C.; Jiang, T.; Wang, S. Hyaluronic acid and carbon dots-gated hollow mesoporous silica for redox and enzyme-triggered targeted drug delivery and bioimaging. *Mater. Sci. Eng. C* **2017**, *78*, 475–484. [CrossRef] [PubMed]
24. Wang, T.; Ma, W.; Shangguan, J.; Jiang, W.; Zhong, Q. Controllable synthesis of hollow mesoporous silica spheres and application as support of nano-gold. *J. Solid State Chem.* **2014**, *215*, 67–73. [CrossRef]
25. Chen, Y.; Xu, P.; Chen, H.; Li, Y.; Bu, W.; Shu, Z.; Li, Y.; Zhang, J.; Zhang, L.; Pan, L.; et al. Colloidal HPMO Nanoparticles: Silica-Etching Chemistry Tailoring, Topological Transformation, and Nano-Biomedical Applications. *Adv. Mater.* **2013**, *25*, 3100–3105. [CrossRef]
26. Chen, Y. *Design, Synthesis, Multifunctionalization and Biomedical Applications of Multifunctional Mesoporous Silica-Based Drug Delivery Nanosystems*; Springer: Berlin/Heidelberg, Germany, 2016.
27. Masalov, V.M.; Sukhinina, N.S.; Kudrenko, E.; Emelchenko, G.A. Mechanism of formation and nanostructure of Stöber silica particles. *Nanotechnology* **2011**, *22*, 275718. [CrossRef]
28. Zhou, X.; Cheng, X.; Feng, W.; Qiu, K.; Chen, L.; Nie, W.; Yin, Z.; Mo, X.; Wang, H.; He, C. Synthesis of hollow mesoporous silica nanoparticles with tunable shell thickness and pore size using amphiphilic block copolymers as core templates. *Dalton Trans.* **2014**, *43*, 11834. [CrossRef]
29. Nguyen, D.H.; Lee, J.S.; Choi, J.H.; Lee, Y.; Son, J.Y.; Bae, J.W.; Lee, K.; Park, K.D. Heparin nanogel-containing liposomes for intracellular RNase delivery. *Macromol. Res.* **2015**, *23*, 765–769. [CrossRef]
30. Tran, D.H.N.; Nguyen, T.H.; Vo, T.N.N.; Pham, L.P.T.; Vo, D.M.H.; Nguyen, C.K.; Bach, L.G.; Nguyen, D.H. Self-assembled poly(ethylene glycol) methyl ether-grafted gelatin nanogels for efficient delivery of curcumin in cancer treatment. *J. Appl. Polym. Sci.* **2019**, *136*, 20. [CrossRef]
31. Nguyen, T.N.; Huynh, T.N.; Hoang, D.; Nguyen, D.H.; Nguyen, Q.H.; Tran, T.H. Functional Nanostructured Oligochitosan–Silica/Carboxymethyl Cellulose Hybrid Materials: Synthesis and Investigation of Their Antifungal Abilities. *Polymers* **2019**, *11*, 628. [CrossRef]
32. Sing, K.S.W.; Everett, D.H.; Haul, R.A.W.; Moscou, L.; Pierotti, R.A.; Rouquerol, J.; Siemieniewska, T. Reporting Physisorption Data for Gas/Solid Systems. *Int. Union Pure Appl. Chem.* **1985**, *57*, 603–619. [CrossRef]
33. Wang, W.; Liu, P.; Zhang, M.; Hu, J.; Xing, F. The Pore Structure of Phosphoaluminate Cement. *Open J. Compos. Mater.* **2012**, *2*, 104–112. [CrossRef]
34. Nguyen, A.K.; Nguyen, T.H.; Bao, B.Q.; Bach, L.G.; Nguyen, D.H. Efficient Self-Assembly of mPEG End-Capped Porous Silica as a Redox-Sensitive Nanocarrier for Controlled Doxorubicin Delivery. *Int. J. Biomater.* **2018**, *2018*, 1575438. [CrossRef] [PubMed]
35. Blanco, E.; Shen, H.; Ferrari, M. Principles of nanoparticle design for overcoming biological barriers to drug delivery. *Nat. Biotechnol.* **2015**, *33*, 941–951. [CrossRef]
36. Shen, S.; Wu, Y.; Liu, Y.; Wu, D. High drug-loading nanomedicines: Progress, current status, and prospects. *Int. J. Nanomed.* **2017**, *12*, 4085–4109. [CrossRef]